

Dynamics of distorted and undistorted soliton molecules in a mode-locked fiber laserJ. Igbonacho,¹ K. Nithyanandan,² K. Krupa,³ P. Tchofo Dinda,^{1,*} P. Grelu,¹ and A. B. Moubissi⁴¹*Laboratoire Interdisciplinaire Carnot de Bourgogne, UMR 6303 CNRS, Université de Bourgogne–Franche-Comté, 9 Avenue A. Savary, Boîte Postale 47870, 21078 Dijon Cedex, France*²*LIPhy Laboratoire Interdisciplinaire de Physique, UMR 5588 CNRS, Université Grenoble Alpes, Saint Martin d'Hères, France*³*Dipartimento di Ingegneria dell'Informazione, Università di Brescia, via Branze 38, 25123 Brescia, Italy*⁴*Département de Physique, Faculté des Sciences, Université des Sciences et Techniques de Masuku, Boîte Postale 943 Franceville, Gabon*

(Received 3 December 2018; published 19 June 2019)

Recent developments in real-time ultrafast measurement techniques have enabled us to prove experimentally that soliton molecules execute internal motions with some aspects similar to those of a matter molecule. Such an analogy between the dynamics of soliton molecules and the dynamics of matter molecules is based on the assumption that the dissipative solitons constituting a molecule are rigid entities sharing a common profile. Whereas this assumption drastically reduces the number of degrees of freedom, it does not hold true in general and we demonstrate that it overlooks some of the essential dynamical features of the soliton molecule. We present a theoretical study based on the principle that the different pulse constituents of a soliton molecule are deformable entities. Specifically, by using of a collective coordinate approach to investigate bi- and trisoliton molecules, we reveal features such as symmetric or asymmetric distortions of their profiles, and energy exchange processes between them. This implies, in subsequent experiments, the use of characterization techniques that can be used to retrieve a larger number of degrees of freedom.

DOI: [10.1103/PhysRevA.99.063824](https://doi.org/10.1103/PhysRevA.99.063824)**I. INTRODUCTION**

In nonlinear photonics, dissipative solitons are light pulses balanced through the interplay among Kerr nonlinearity, dispersion and/or diffraction, and nonlinear gain and loss [1,2]. By combining integrated optical components in a compact tabletop format, ultrafast fiber lasers constitute a versatile platform to generate temporal dissipative solitons and investigate their wide range of complex dynamics and pattern formations [2,3]. Among complex nonlinear dynamics, multiple pulse operation has been attracting a great amount of interest over the past 20 years, both theoretically and experimentally [4–7]. With the increase of the laser pumping power, a single pulse will generally accumulate an excessive nonlinear phase shift during the cavity round trip, which results in a multipulsing instability [8–10]. In the case of an additive-pulse mode-locking scheme, such as in the popular nonlinear polarization evolution (NPE) mode locking, the instability can take the form of an overdrive of the virtual saturable absorber [11]. The multipulsing instability can also result from the interplay between spectral filtering, self-phase modulation, and chromatic dispersion [12–14]. Nevertheless, in spite of the intertwined physical effects promoting the multipulsing instability, the transition toward the multipulse operation can be viewed as a dynamical response of the laser to regain stability at an increased pumping power, with the intracavity energy being shared equally among a larger number of pulses [15]. Such an equal share is explained by the presence of a dynamical attractor of focus type: as long as the pulses remain sufficiently sep-

arated, they adopt a unique field profile, defined by the attractor, and therefore they will carry the same energy [4,16]. This results in the so-called “soliton energy quantization,” which has been observed and modeled years ago [17,18], and is in fact a clear manifestation of the dissipative soliton attractor.

Among the wide range of multipulse dynamical structures investigated so far, “soliton molecules” have attracted a considerable interest. A soliton molecule (SM) is a bound state of several interacting solitons that are separated typically by a few pulse widths [4,19–29]. Composed of two bound solitons, the soliton pair, also termed a bisoliton molecule, can be viewed as the most fundamental SM, whose dynamical properties can be extrapolated to a large extent to SMs with more constituents pulses [4,11,30]. As a result of the pulse interactions, the pulses’ relative separations and phases can self-lock, resulting in ultrastable pulse patterns of sub-femtosecond timing jitter [31]. Due to their high stability, SMs have been considered as possible symbols of a multilevel modulation format for fiber-optic communication systems [32,33]. Extending further the analogy between SMs and matter molecules, it was discovered that a bi-SM could also vibrate [34]. The early experimental investigations were supported by numerical simulations that showed how the relative temporal separation and phase would oscillate over successive cavity round trips, highlighting the existence of various attractors of limit-cycle type. Thus, besides vibrating soliton pairs [34,35], an oscillating phase [36], a flipping phase (switching between in-phase and out-of phase states) [37,38], and an independently evolving phase [26,39] were unveiled. The numerical exploration of these SM dynamics involved different models, featuring various dispersion maps and additional effects such as gain saturation, fast or slow gain dynamics,

*tchofo@u-bourgogne.fr

and instantaneous or noninstantaneous saturable absorbers. Such a wide exploration has demonstrated the universality of pulsating and vibrating SMs within ultrafast laser systems.

Until recently, laser oscillators having typical repetition rates in the 10s of MHz were lacking a real-time single-shot characterization. Therefore, the nonstationary SM dynamics introduced above were only weakly supported experimentally by the use of averaged data. A major turn came in the last few years with the development of the time-stretch dispersive Fourier transform (DFT) method [40], enabling the recording of successive laser output optical spectra at unprecedented frame rates. This allowed us to obtain strong experimental proof of the existence of a variety of vibrating and oscillating SMs [38,41–43].

Different levels of characterization of SMs are possible. At the simplest level, a bi-SM is defined by the peak-to-peak separation τ and the relative phase $\Delta\phi$ between the two pulses. The various robust SMs introduced above, from stationary to oscillating ones, were predominantly classified based on their evolution trajectories in the phase plane consisting of these two internal degrees of freedom, called the interaction plane [44]. In recent experiments, these two degrees of freedom, τ and $\Delta\phi$, were retrieved from each recorded optical spectrum of a large set corresponding to successive cavity round trips, yielding a clear identification of the dynamical evolution [41,42,45].

We now raise two points that are essential for a better understanding of the dynamical possibilities of SMs. First, basing the dynamical analysis on the parameters τ and $\Delta\phi$ provides only a partial description of the internal dynamics of the SM, where the solitons making up the molecule are treated as rigid bodies. As mentioned earlier, this is based on the assumption that, when the pulses are a few pulse widths apart, a strong dissipative soliton attractor will provide an identical profile to each pulse. Whereas this works in essence for the stationary SM, this would just be a lower-order approximation in the case of a nonstationary SM. For SM formed by closely separated pulses, featuring a strong overlap, this approximation is unlikely to hold true. Therefore, a better exploration of the possible dynamical behavior of SMs necessitates treating the soliton constituents as deformable entities. For the experimental counterpart, this implies implementing a real-time characterization technique able to retrieve a sufficiently comprehensive set of internal degrees of freedom [46,47]. As a second point, we also investigate tri-SM dynamics. Whereas in the model of identical solitons an additional soliton in the molecule would increase the number of internal degrees of freedom by 2—the additional relative phase and temporal separation—even more complex dynamical behavior can be anticipated with deformable pulses.

In the present study, we investigate numerically the internal dynamics of SMs in a mode-locked fiber laser by means of a collective-coordinate approach, which is based on the following major soliton parameters: energy, peak power, temporal width, spectral width, and frequency chirp. This approach reveals that the internal dynamics of SMs can be accompanied by symmetric or asymmetric distortions of their intensity profiles, inducing energy exchange between solitons, and modifications of all the above-mentioned soliton parameters.

The paper is organized as follows: Section II describes the analytical collective-coordinate characterization methods of SMs. Section III presents the numerical model employed for the simulation of the cavity dynamics. In Sec. IV, we present the major features of the dynamics of bi- and tri-SMs obtained for nondeformable individual soliton constituents, while Sec. V presents the dynamics of molecules with deformable solitons. In Sec. VI we include the experimental observation of a phase-oscillation dynamics for a tri-SM. Section VI concludes the paper with a summary of our results.

II. CHARACTERIZATION METHODS OF SOLITON MOLECULE DYNAMICS

A SM can be characterized and analyzed at qualitatively distinct levels of detail. The basic level of characterization consists in treating each of the solitons within a SM as a nondeformable entity [41,42]: the dynamical behavior of each soliton is described by two parameters corresponding to its temporal position and its temporal phase, while the dynamical state of the whole SM is characterized by the evolution of the temporal separations and the phase differences among solitons. The appeal of this approach is that it provides a general overview of the way the solitons move in relation to each other. However, this basic level of characterization is rigorously relevant only in cases in which all the solitons of the SM have the same intensity profile, as schematically represented in Fig. 1(a) for the case of a bisoliton. When strongly interacting dissipative solitons undergo complex internal dynamics, they are likely to behave as deformable entities. In general, considering the dissipative nature of the dynamical system, the interactions among the dissipative solitons that form a SM are of an inelastic nature, resulting in significant transient distortions of their intensity profiles, even though some dynamical evolutions can mimic the appearance of conservative dynamics [48,49]. The intensity profile of a distorted bisoliton molecule is schematically illustrated in Fig. 1(b), featuring significant differences between the peak powers (P_1, P_2) and temporal widths (ξ_1, ξ_2) of the two solitons making up the SM. It is clear from Fig. 1(b) that, to appropriately analyze the internal dynamics of a distorted SM, it is necessary to use a higher level of characterization taking into account the greater number of degrees of freedom that can be excited by the inelastic interactions among solitons in the SM.

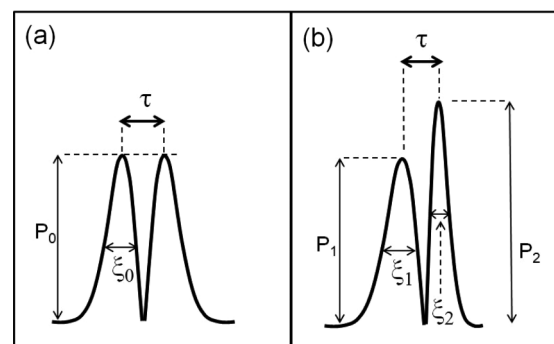


FIG. 1. Schematic of the temporal intensity profile of a bisoliton molecule: (a) undistorted and (b) distorted.

The characterization of the internal dynamics of a complex system having a large number of degrees of freedom requires an elaborate approach such as the collective coordinate approach developed in Refs. [50–53]. The idea is to associate to each relevant degree of freedom a variable called a collective coordinate (CC), which is introduced in the theoretical treatment through a trial function, known as the ansatz function. As long as the solitons are sufficiently separated from each other, to be considered as distinct entities, a satisfactory choice for the ansatz (electric-field envelope) of a SM may simply be formulated as follows:

$$f = \sum_{i=1}^N g_i \quad \text{with} \quad g_i \equiv X_{1i} \exp \left[-\frac{(t - X_{2i})^2}{X_{3i}^2} \right] \times \exp i \left[\frac{X_{4i}}{2} (t - X_{2i})^2 + X_{5i} (t - X_{2i}) + X_{6i} \right], \quad (1)$$

where the labels $i = 1, 2, 3, \dots$ denote, respectively, the solitons constituting the SM. Hereafter, we will focus on bi- ($N = 2$) and tri- ($N = 3$) SMs. The CCs X_{1i} , X_{2i} , X_{3i} , X_{4i} , X_{5i} , and X_{6i} are, respectively, the amplitude, temporal position, temporal width, chirp, central frequency, and the phase constant of the soliton labeled “ i .” CCs allow us to obtain more practical parameters: the peak power $P_i \equiv X_{1i}^2$, the temporal width $\xi_i \equiv \sqrt{2 \ln(2)} X_{3i}$, the chirp $C_i \equiv X_{4i}/2$, and the spectral width $\Delta \nu_i \equiv \frac{\sqrt{2(4 + X_{4i}^2 X_{3i}^4) \ln(2)}}{2\pi X_{3i}}$. It is worth noting that the choice of an ansatz function is necessary to describe the internal dynamics of any nonintegrable system, but the ansatz corresponds to an approximation whose quality level depends on the magnitude of the residual field defined by $q \equiv |\psi - f|$, ψ being the exact field solution (accessible only numerically). Once the ansatz function is defined, the CC approach can be performed in several ways that differ considerably in their respective levels of complexity, according to the number of CCs considered. In this regard, previous work has highlighted the following important facts [52]:

(i) As long as the number of degrees of freedom is sufficiently small, i.e., less than or equal to 6, the internal dynamics of a solitonic structure can be described by a set of first-order ordinary differential equations (ODEs), which give the analytical expression of the velocity of each CC as a function of the CCs [52]. This set of ODEs, which are referred to as the *variational equations*, has the great advantage of showing explicitly how each of the propagation phenomena (dispersion, nonlinearity, losses, etc.) modifies the CCs of the solitonic structure. However, this advantage is obtained at the cost of an approximation (called a *bare approximation* [52]), which is to totally ignore the residual field. However, in general, the variational equations give a quite satisfactory qualitative description of the internal dynamics of nonintegrable systems.

(ii) Reference [52] showed that in a nonintegrable system with a very large number of degrees of freedom (i.e., more than 6 CCs), variational equations become too tedious and virtually unusable.

The analytical expression of our ansatz (1), i.e., with, respectively, 12 and 18 CCs for the bi- and tri-solitons molecules, is formulated to allow detection of a possible asymmetry in the profile of a soliton molecule. But the large number of CCs that is used makes the variational approach

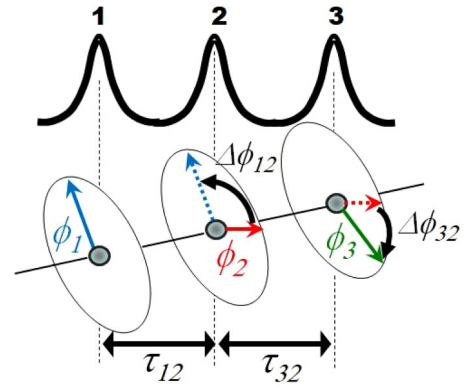


FIG. 2. Coordinates used in the characterization of trisoliton molecule dynamics when soliton pulses remain undistorted.

virtually unworkable. Consequently, in the present work we use a much more convenient characterization procedure, which is to minimize the energy of residual field, which has been shown to be equivalent to the full CC approach (in which the equations of motion of the CCs are coupled to an equation giving the evolution of the residual field [52]). The residual field minimization method is a two-step procedure. First, we determine the exact electric field of the SM, ψ , by solving the equations of intracavity dynamics presented in the following section. Then we determine the set of CCs (X_{ij} ; $i = 1, 2, \dots, 6$; $j = 1, 2$) for which the ansatz f defined by Eq. (1) is the best representation of the exact field ψ . This is equivalent to determining the set of CCs that minimize the residual field energy defined by $E_{RF} = \int_{-\infty}^{+\infty} |q|^2 dt$.

We can easily extend the notations used for a bi-SM to the case of a tri-SM. The successive solitons are labeled 1, 2, and 3, as shown in Fig. 2 for the case of undistorted solitons that will be investigated in Sec. IV. Here, the notation $\Delta \tau_{12}$ ($\Delta \tau_{32}$) designates the temporal separation between solitons 1 and 2 (3 and 2). $\Delta \phi_{12} = \phi_1 - \phi_2$ ($\Delta \phi_{32} = \phi_3 - \phi_2$) denotes the relative phases between solitons, where ϕ_1 , ϕ_2 , and ϕ_3 stand for the phases of solitons 1, 2, and 3, respectively.

III. NUMERICAL MODEL

Our modeled laser architecture is shown in Fig. 3. It represents a dispersion-managed fiber ring laser cavity, which comprises an erbium-doped fiber (EDF) with normal

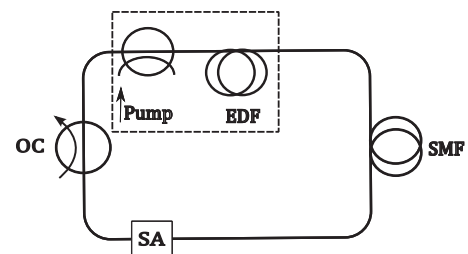


FIG. 3. Schematic of the fiber laser cavity. EDF: erbium-doped fiber; SMF: passive single-mode fiber; SA: ultrafast saturable absorber; OC: output coupler. The fiber ring laser operates in the unidirectional propagation mode, clockwise in the figure.

dispersion at $1.55 \mu\text{m}$ (amplifier medium), a section of single-mode fiber (SMF) with anomalous dispersion, a saturable absorber (SA), and an output coupler (OC).

We use a lumped propagation model in which each component of the cavity is modeled by a separate equation, and the pulse propagation follows a concatenated sequence representing the different cavity elements. The pulse propagation in the fiber system is modeled by a generalized nonlinear Schrödinger equation in the following form [54]:

$$\frac{\partial \psi}{\partial z} + \frac{i}{2} \beta_2 \frac{\partial^2 \psi}{\partial t^2} - \frac{g}{2} \psi = -\frac{\alpha}{2} \psi + i\gamma |\psi|^2 \psi, \quad (2)$$

where ψ is the slowly varying electric field in the retarded frame of reference moving at the group velocity. γ , β_2 , g , and α are the Kerr nonlinearity, dispersion, gain, and attenuation coefficients, respectively. For the passive fiber (SMF), $g = 0$, whereas for the active fiber (EDF) $g \equiv g(z, P_{\text{av}}, \omega_s)$, which is calculated at the signal frequency ω_s , as a function of the propagation distance z and the average power P_{av} at the input facet of the EDF. The value of P_{av} is related to the total field energy E as follows: $P_{\text{av}}(z) \equiv \frac{E(z)}{\tau_{\text{RT}}} = \frac{1}{\tau_{\text{RT}}} \int_{-\infty}^{\infty} |\psi(t, z)|^2 dt$, where τ_{RT} designates the cavity round-trip time. The procedure for calculating $g(z, P_{\text{av}}, \omega_s)$ is detailed in Ref. [13].

The action of SA is modeled by the following instantaneous transfer function: $P_o = T P_i$, where $T \equiv T_0 + \frac{\Delta T P_i}{P_i + P_{\text{sat}}}$ describes the transmission of the SA, and T_0 and ΔT are the reflectivity and modulation depth of the SA. P_i (P_o) is the instantaneous input (output) optical power, while P_{sat} is the saturation power. The other lumped elements of the laser cavity (coupler, fiber splices) only affect the pulse amplitude linearly.

We used the following typical parameters for the fiber cavity elements:

(i) EDF: $\gamma = 3.6 \times 10^{-3} \text{ W}^{-1} \text{ m}^{-1}$; length $L_{\text{EDF}} = 4.5 \text{ m}$; $\beta_2 = 16 \text{ ps}^2/\text{km}$. The parameters used for the calculation of the gain provided by the EDF (core radius, doping radius, doping concentration of erbium ions, absorption and emission cross section, etc.), are taken from Ref. [13].

(ii) SMF: $\gamma = 1.3 \times 10^{-3} \text{ W}^{-1} \text{ m}^{-1}$; $\beta_2 = -21.7 \text{ ps}^2/\text{km}$; $A_{\text{eff}} = 78.5 \mu\text{m}^2$. We use a fiber length $L_{\text{SMF}} = 3.3 \text{ m}$, so that the average second-order dispersion is null.

(iii) SA: $T_0 = 0.70$, $\Delta T = 0.30$, $P_{\text{sat}} = 10 \text{ W}$.

IV. SOLITON MOLECULE DYNAMICS BASED ON UNDISTORTED SOLITON CONSTITUENTS

In what follows, we use numerical simulations to study bi- and tri-SMs within the laser cavity and characterize their internal motion. Our procedure for generating tri-SMs is to explore point by point, with a very fine discretization step, a two-dimensional parameter space, in which one of the parameters is the pump power of the gain medium, P_p , while the other parameter is the saturation power of the SA, P_{sat} . For each set of parameters (P_p , P_{sat}), we simulate the evolution of the intracavity field starting from an initial condition corresponding to photon noise. If the intracavity field converges to a multipulse stable state, then we proceed to its characterization to verify if this stable state is a SM.

The basic level of characterization is based on the following two points:

- (i) The evolution of the intensity profile of the intracavity field as a function of the number of cavity round trips.
- (ii) The analysis of the temporal separations and the relative phases between solitons.

In a pool of different parametric spaces, we have found some regions where the trisoliton molecules exhibit behaviors similar to those known for bisoliton molecules, while in other regions we find qualitatively different behaviors. In this context, it should be noted that the previous work has highlighted the existence of parameter regions where bisoliton molecules propagate without internal dynamics, and other regions where bisolitons exhibit a diversity of behaviors that can be broadly classified into three categories:

- (i) The *phase oscillation*, which designates a dynamic where the relative phase between solitons executes oscillations, while the temporal separations vary only marginally.
- (ii) The *vibration of molecule*, which corresponds to a bound state where the relative phases and temporal separations oscillate simultaneously.
- (iii) The *phase drift*, which refers to a case characterized by an unbound variation of phase, without oscillations.

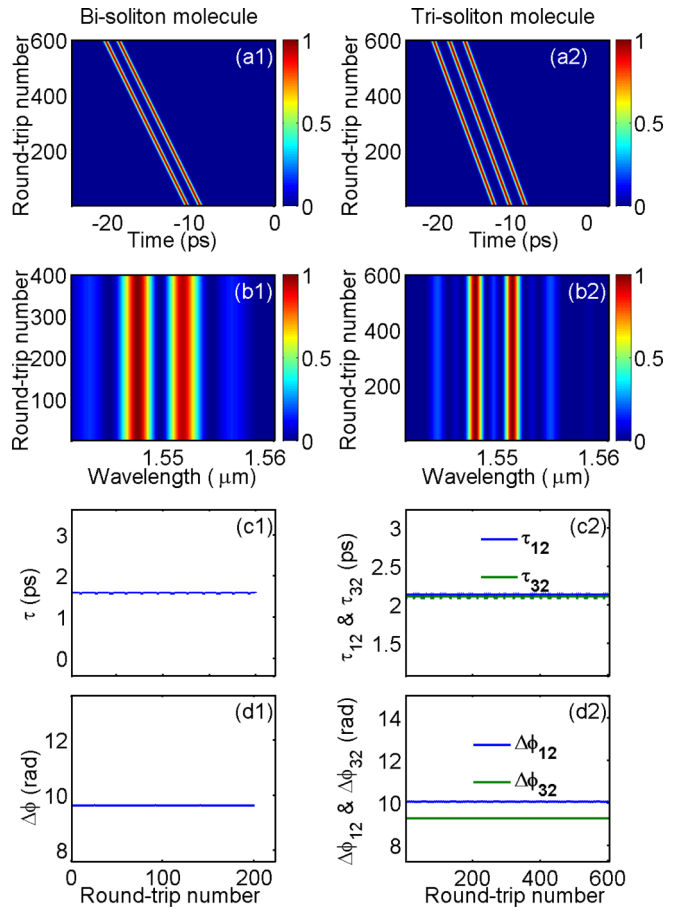


FIG. 4. Stationary dynamics of SMs. (a1),(a2) 2D contour of the temporal intensity. (b1),(b2) 2D contour of the spectral intensity. (c1),(c2) Temporal separations. (d1),(d2) Relative phases. The two-soliton molecule [(a1), (b1), (c1), and (d1)] and trisoliton molecule [(a2), (b2), (c2), and (d2)] are generated using ($P_p = 43.5 \text{ mW}$, $P_{\text{sat}} = 6 \text{ W}$) and ($P_p = 50 \text{ mW}$, $P_{\text{sat}} = 2 \text{ W}$), respectively. $T_0 = 0.7$ and $\Delta T = 0.3$.

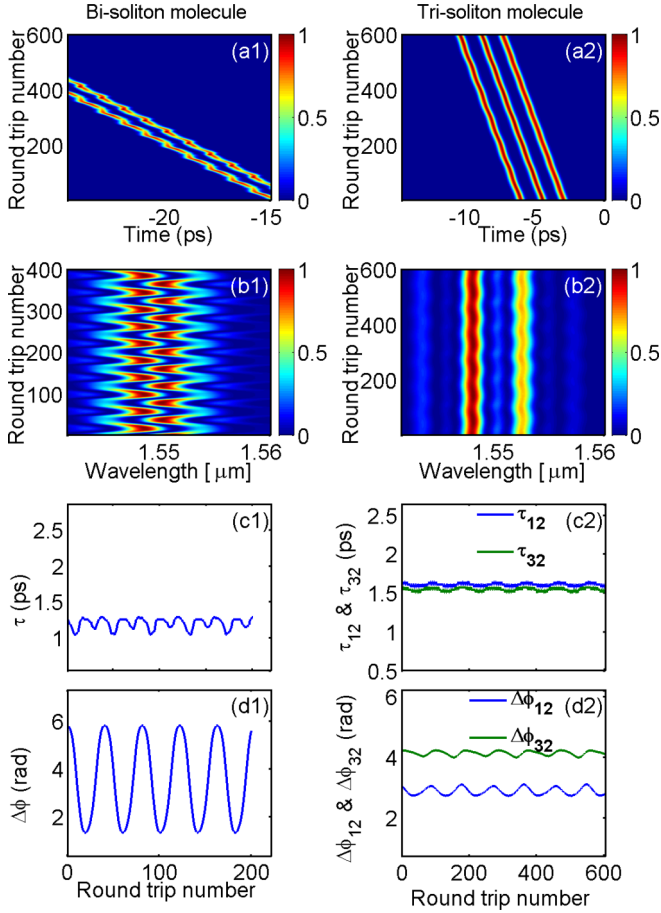


FIG. 5. Dynamics with phase oscillations. (a1),(a2) 2D contour of the temporal intensity. (b1),(b2) 2D contour of the spectral intensity. (c1),(c2) Temporal separations. (d1),(d2) Relative phases. The two-soliton molecule [(a1), (b1), (c1), and (d1)] and trisoliton molecule [(a2), (b2), (c2), and (d2)] are generated using ($P_p = 47.5$ mW, $P_{\text{sat}} = 10$ W) and ($P_p = 61$ mW, $P_{\text{sat}} = 4$ W), respectively. The other system parameters are the same as in Fig. 4.

Thereafter, in all cases in which the trisoliton exhibits a behavior similar to that of a bisoliton, we will put side-by-side the results of the two types of molecule in order to facilitate the comparison.

A. Stationary dynamics

Figure 4 demonstrates that our laser cavity can generate bisoliton and trisoliton molecules propagating in the stationary regime, respectively, for the following sets of parameters: ($P_p = 43.5$ mW, $P_{\text{sat}} = 6$ W) and ($P_p = 50$ mW, $P_{\text{sat}} = 2$ W). This regime corresponds to a fixed point of the slow dynamics, i.e., a regime in which, for any location within the cavity, the temporal separations and the relative phases between solitons take the same values after each cavity round trip.

B. Phase oscillations

Figure 5 shows that for ($P_p = 47.5$ mW, $P_{\text{sat}} = 10$ W) and ($P_p = 61$ mW, $P_{\text{sat}} = 4$ W), the laser cavity generates bisoliton and trisoliton molecules, respectively, with internal dynamics mainly dominated by oscillations of the relative

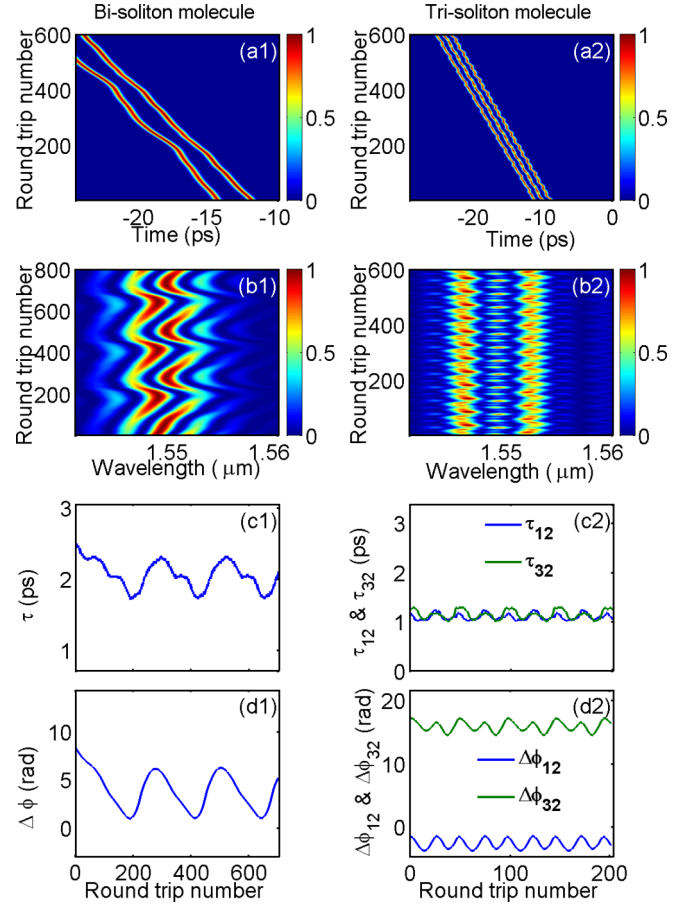


FIG. 6. Vibrations of SMs. (a1),(a2) 2D contour of the temporal intensity. (b1),(b2) 2D contour of the spectral intensity. (c1),(c2) Temporal separations. (d1),(d2) Relative phases. The two-soliton molecule [(a1), (b1), (c1), and (d1)] and trisoliton molecule [(a2), (b2), (c2), and (d2)], are generated using ($P_p = 42.5$ mW, $P_{\text{sat}} = 9$ W) and ($P_p = 74$ W, $P_{\text{sat}} = 6$ W), respectively. The other system parameters are the same as in Fig. 4.

phases between solitons [see Figs. 5(d1) and 5(d2)]. Within this dynamics, the temporal separations between solitons execute relatively small-amplitude motions around a stable configuration as shown in Figs. 5(c1) and 5(c2).

C. Internal vibrations

Figure 6 shows that the laser cavity under consideration can generate bisoliton and trisoliton molecules whose internal dynamics are characterized by large-amplitude oscillations for both the separations between solitons and their relative phases. This type of dynamics is one of the most frequently observed within our cavity model. The results of Fig. 6 were obtained for ($P_p = 42.5$ mW, $P_{\text{sat}} = 9$ W) for the bisoliton, and ($P_p = 74$ mW, $P_{\text{sat}} = 6$ W) for the trisoliton.

D. Dynamics with linear phase drift

In certain parameter regions, bisoliton molecules will follow a dynamical behavior characterized by an unbound drift of the relative phase between the two solitons [26,39,41]. Here, we find trisoliton molecules following similar

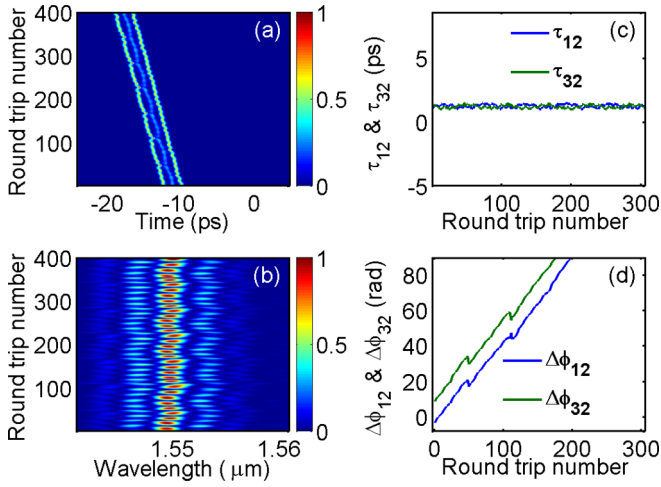


FIG. 7. Tri-SM dynamics with unbound phase drift, obtained for $P_p = 52$ mW and $P_{\text{sat}} = 2$ W. (a) 2D contour of the temporal intensity. (b) 2D contour of the spectral intensity. (c) Temporal separation. (d) Relative phase. The other system parameters are the same as in Fig. 4.

dynamics. Figure 7, which we obtained for $P_p = 52$ mW and $P_{\text{sat}} = 2$ W, illustrates a situation in which the leading and the trailing solitons evolve with a similar relative phase dynamics with respect to the central soliton. This phase dynamics is an unbound drift, characterized by a major linear trend.

E. Dynamics with bounded phase drift

Despite the existence of many similarities in their behaviors, there should be some qualitative differences between some bisoliton and trisoliton molecule dynamics. Figure 8, which we obtained for $P_p = 62$ mW and $P_{\text{sat}} = 5$ W, illustrates an internal dynamics that has not been observed so far in the behavior of bisoliton molecules. This dynamics is

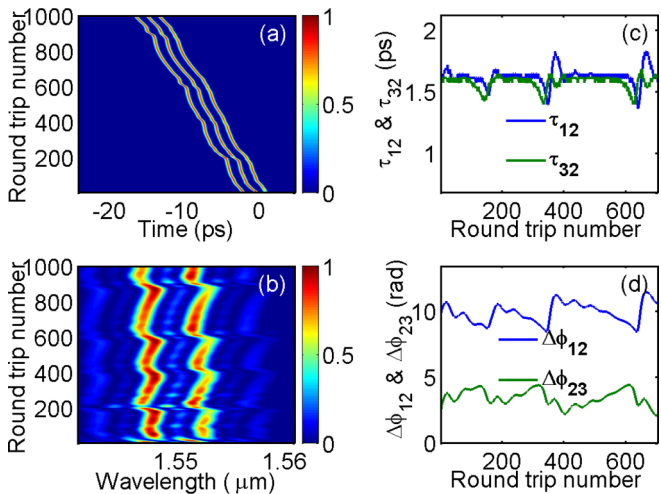


FIG. 8. Tri-SM dynamics with bound phase drift, obtained for $P_p = 62$ mW and $P_{\text{sat}} = 5$ W. (a) 2D contour of the temporal intensity. (b) 2D contour of the spectral intensity. (c) Temporal separation. (d) Relative phase. The other system parameters are the same as in Fig. 4.

characterized by a complex phase evolution that combines a quasilinear drift with a low-amplitude oscillation, followed by a steep phase back-drift that occurs quasiperiodically. Such evolution includes chaotic fluctuations on an overall bounded phase-drift dynamics.

V. DEFORMABLE SOLITON MOLECULES

In the previous section, we have shown that our cavity can generate a great diversity of bi- and tri-solitons that can be classified according to dynamical features easily distinguishable from each other on the basis of the evolution of two of the soliton parameters, namely their temporal position and their phase. However, to enlarge our vision of possible SM dynamics, we need to characterize them according to the possible evolution of the parameters having a direct link with the intensity profile of each soliton, such as the soliton’s energy, peak power, or temporal width. In what follows, we show that the collective-coordinate approach presented in Sec. II provides valuable details on the intensity profile of each of the solitons that make up a SM. The most unexpected result is the possible existence of SMs having an intrinsically distorted intensity profile, i.e., with strong inequalities in the energies, peak powers, or temporal widths of solitons within the same SM, which evolve along with the propagation distance.

A. Deformable bisolitons

Figure 9 shows the dynamical behavior of a SM modeled for the pump power $P_p = 47.5$ mW and the following parameters for SA: $T_0 = 0.7$, $\Delta T = 0.3$, and $P_{\text{sat}} = 16$ W. Figure 9(a), which we obtained for a propagation up to 10 000 cavity round trips, shows that the dynamics of this SM follows a circular trajectory in the phase plane represented by $\tau \cos(\Delta\phi)$ versus $\tau \sin(\Delta\phi)$. This SM has as a major characteristic the displaying of an oscillation of the separation between solitons [see Fig. 9(b)] while the relative phase drifts linearly [see Fig. 9(c)]. However, when we investigate the presented dynamics more carefully, we can clearly observe that this SM is highly distorted. Indeed, Fig. 9(d) shows that the respective energies of the two solitons oscillate around average values that differ by about 30%. Specifically, this SM has an asymmetric overall intensity profile. Indeed, one can notice in Fig. 9(h) that the gap between the average values of the respective temporal widths of the two solitons is rather low; this indicates that the large difference in energy between the two solitons results mainly from a large gap between their respective peak powers (which exceeds 30%), as Fig. 9(f) shows. Furthermore, the asymmetry of this SM also appears in the chirp and the spectral width, as shown in Figs. 9(g) and 9(i).

As we have shown in Figs. 5(a1), 5(b1), 5(c1), and 5(d1), by choosing a pump power of 47.5 mW for the gain medium, and the parameter $P_{\text{sat}} = 10$ W for the SA, the cavity generates a bisoliton having mainly a dynamic with phase oscillations. In this respect, it should be recalled that the results in Fig. 5 were obtained by applying to the bisoliton a basic characterization method using solely two degrees of freedom corresponding, respectively, to the temporal position and the temporal phase of the soliton, deduced directly from the

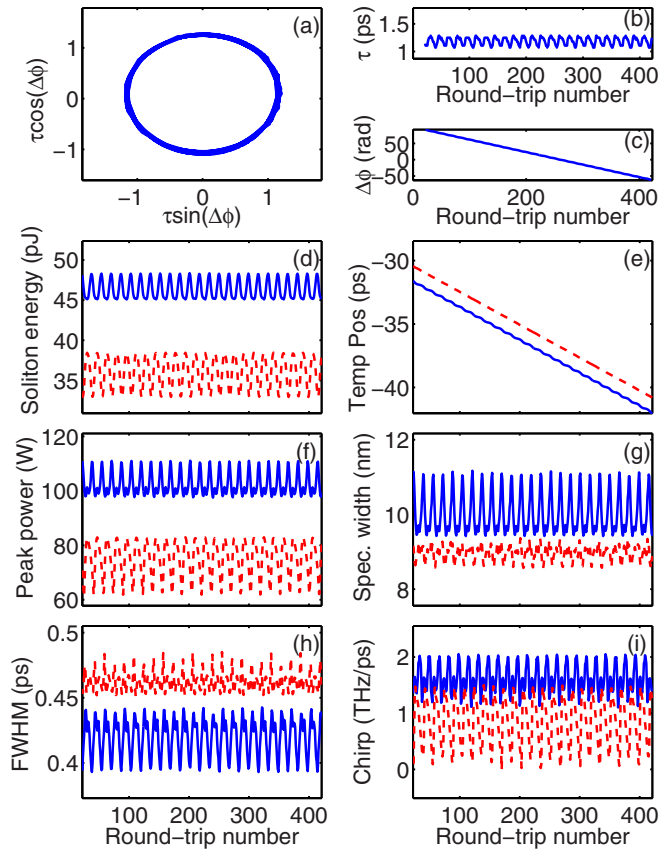


FIG. 9. Distorted bisoliton molecule: evolution of the parameters for each soliton as a function of cavity round trips for $P_p = 47.5$ W, $P_{\text{sat}} = 16$ W. (a) Trajectory of the dynamics in the phase plane. (b) Temporal separation. (c) Relative phase. (d) Soliton energy. (e) Temporal position. (f) Peak power. (g) Spectral width. (h) Temporal FWHM (full width at half-maximum). (i) Chirp.

temporal profile of the intracavity field. Figure 10 shows the results obtained by applying to the bisoliton of Fig. 5 the characterization approach using eight collective coordinates instead of two. The results displayed in Figs. 10(a), 10(b) and 10(c) are consistent with those from Figs. 5(c1) and 5(d1), with the trajectory of this bisoliton in the two-dimensional phase plane following the shape of a crescent; see Fig. 10(a). The temporal separation (temporal phase) oscillates with a relatively small (large) amplitude, as shown in Figs. 10(b) and 10(c), with an oscillation period around 40 cavity round trips. In addition, the advantage of the CC approach appears clearly in the panels (d)–(i) of Fig. 10, which reveal valuable unsuspected details on the individual behavior of each of the solitons of this bisoliton. Panels (d)–(i) of Fig. 10, showing the evolution of the corresponding parameters of each soliton of the SM, highlight characteristics that are qualitatively different from those of the asymmetric SM shown in Fig. 9. Figure 10(d) shows that the respective energies of the two solitons of this SM oscillate around the same average value. This indicates that this SM executes internal dynamics around a symmetrical intensity profile. Each soliton deforms very strongly, in a periodic manner, with the same period as that of the oscillations of the SM in the phase plan (τ , $\Delta\phi$). We notice from Fig. 4(d) a marked energy exchange between the two

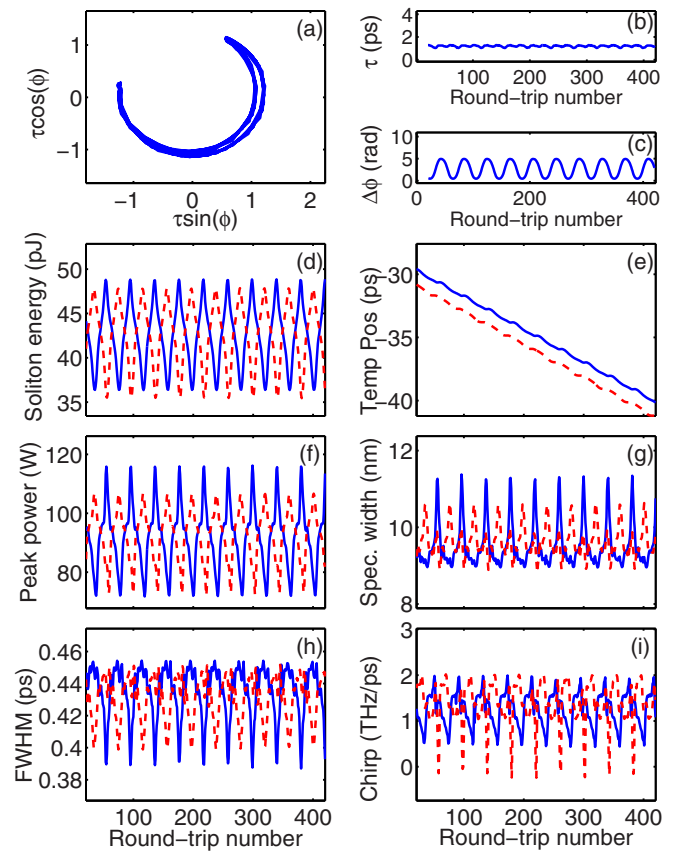


FIG. 10. Deformable two-SM: evolution of the soliton parameters as a function of cavity round trips for $P_p = 47.5$ W, $P_{\text{sat}} = 10$ W. (a) Trajectory of the dynamics in the phase plane. (b) Temporal separation. (c) Relative phase. (d) Soliton energy. (e) Temporal position. (f) Peak power. (g) Spectral width. (h) Temporal FWHM. (i) Chirp.

solitons forming the bound state, which reflects the inelastic interaction between them. The curves of the peak power and the temporal width [Figs. 10(f) and 10(h)] give additional insight into the way in which each soliton deforms during propagation. Indeed, the peak power and the temporal width of each soliton vary in opposite directions, which leads to an alternation of processes of temporal shrinking and broadening of the intensity profile of the soliton, namely a breathing phenomenon.

Thus, Figs. 10(f) and 10(h) show both solitons execute a breathing motion in an almost out-of-phase fashion. The other parameters of the soliton (spectral width and chirp) oscillate in a similar way.

B. Deformable trisolitons

Figure 11, which correspond to the results presented in Fig. 6 (for $P_p = 74$ mW and $P_{\text{sat}} = 6$ W), provides deep insight into the internal dynamics of a trisoliton molecule by highlighting the individual dynamic behavior of each of the constituents of the molecule.

This tri-SM has nearly a symmetrical intensity profile, because the two side solitons (the leading and trailing ones) experience similar oscillations, as illustrated by Figs. 11(a),

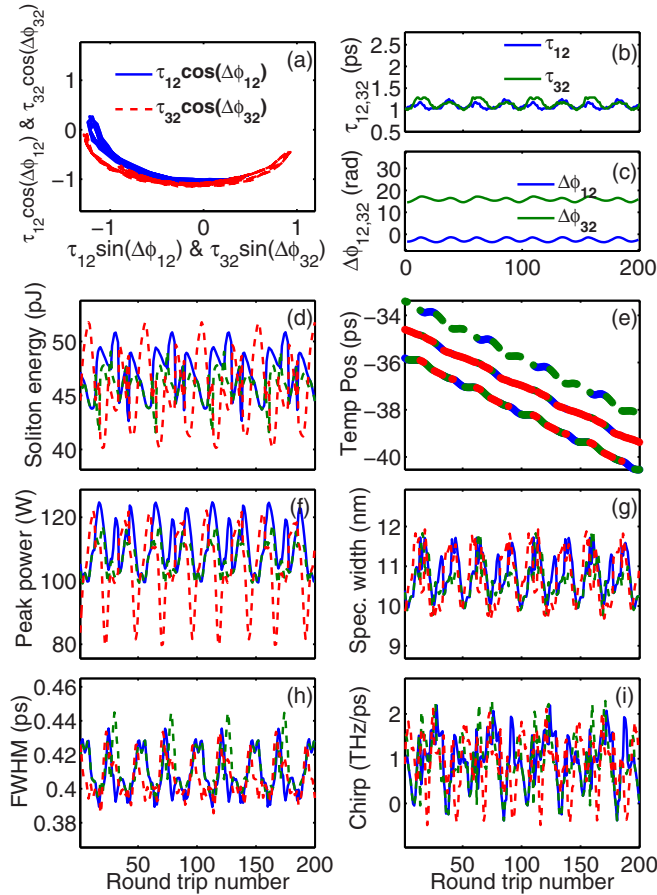


FIG. 11. Deformable tri-SM: evolution of the soliton parameters as a function of cavity round trips for $P_p = 74$ mW, $P_{sat} = 6$ W. (a) Trajectory of the dynamics in the phase plane. (b) Temporal separation. (c) Relative phase. (d) Soliton energy. (e) Temporal position. (f) Peak power. (g) Spectral width. (h) Temporal FWHM. (i) Chirp.

11(b), and 11(c). Moreover, Fig. 11(d) unveils that the respective energies of the three solitons vary virtually around the same average value. Furthermore, Fig. 11(d) shows that the amplitude of oscillations of the energy of the central soliton is almost twice as large as that of each of the side solitons. In addition, we observe that the energy of the central soliton reaches its maximum value when the energies of the side solitons are at their minimum values. These observations clearly indicate a process of exchange of energy between the central soliton and the two side solitons, thus confirming the idea that SMs behave as entities consisting of deformable constituents. In this respect, it should be emphasized that, although the intensity profile of this trisoliton is intrinsically symmetrical, the different solitons of the molecule do not deform in the same way. Figures 11(d) and 11(f) show that the central soliton is the one that experiences maximum profile distortion, with a range of variation of its energy that represents almost 25% of its minimum value (~ 40 pJ), while the range of variation of its peak power reaches almost 50% of its minimum value (~ 80 W). The respective temporal widths of these solitons also vary, but in very moderate proportions, by about 8%, as shown in Fig. 11(h). Qualitatively, by comparing the

variations of the peak power [Fig. 11(f)] with those of the temporal width [Fig. 11(h)], one can deduce that these deformations correspond to a breathing phenomenon. Indeed, when the peak power of the soliton increases, its temporal width decreases, and vice versa. It can also be noted that the internal dynamics of the soliton affect all the parameters of the SM, including its spectral width [Fig. 11(g)] as well as the chirp [Fig. 11(i)].

VI. PRELIMINARY EXPERIMENTAL RESULTS

One of the highlights of the above numerical simulations is the amazing diversity of dynamical light structures that can be generated within a fiber laser cavity. Recent experimental works have clearly demonstrated the generation of a variety of bisolitons dynamics [41,42,45]. The natural continuation of those experimental works should be the exploration of the internal dynamics of trisolitons. In [42], the dynamics of a tri-SM with unbounded phase drift was analyzed experimentally. In what follows, we present the experimental demonstration of generation of a tri-SM with oscillating phase dynamics. We use the experimental setup reported in Ref. [41]. It consists of a 1.55 m fiber laser with a total cavity length of 4.43 m, composed of a 0.55-m-long erbium-doped silica fiber (EDF, 110 dB/m absorption at 1530 nm), backward-pumped by a 980 nm laser diode (LD), and of 3.45-m-long standard single-mode fibers (SMFs-28). The total cavity dispersion is anomalous with $\beta_2 = -17.84$ ps² km⁻¹. A polarization-insensitive optical isolator ensures the unidirectional light propagation. The laser is mode-locked by using nonlinear polarization evolution (NPE) in the fibers followed by discrimination with a polarizing beam splitter (PBS), controlled by the orientations of wave plates. The experimental characterization is performed through the 50/50 fiber coupler. The DTF was implemented by temporally stretching the laser output in around a 1.3-km-long dispersion compensating fiber (DCF), and recording the

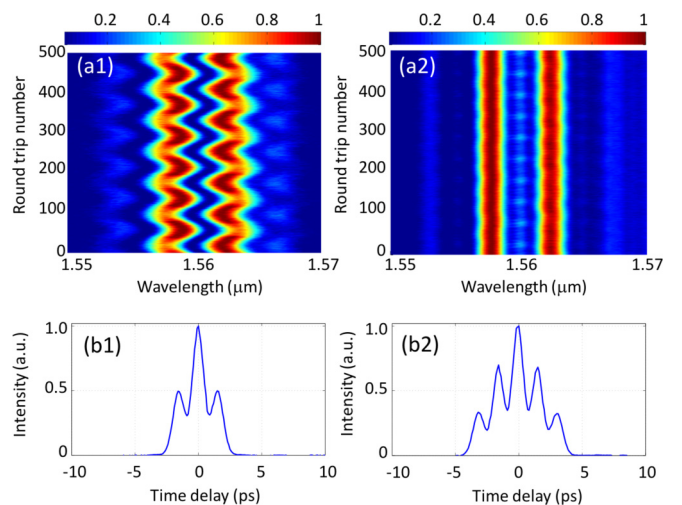


FIG. 12. Experimental observations of bisoliton (a1),(b1) and trisoliton (a2),(b2) molecule dynamics featuring oscillating phase; (a1),(a2) 2D contour plot of 500 consecutive single-shot spectra obtained from real-time DFT measurement; (b1),(b2) normalized multi-shot second-order autocorrelation trace; pump power = 285 mW.

resulting temporal waveform by a 6-GHz ultrafast oscilloscope via a high-speed 45-GHz photodiode. NPE provides a virtual, quasi-instantaneous, saturable absorber effect whose transfer function can be tuned by adjusting the orientations of the wave plates. As a consequence, numerous different operation regimes can be accessed in a reproducible way. However, it is worth noting that at a practical level, the generation of soliton molecules requires a very careful adjustment of the transfer function, which is a delicate and tedious operation, especially when exciting bound states comprising more than two solitons. Figure 12 shows a preliminary experimental result of the real-time observation of the internal dynamics of tri-SM with oscillating phase, which can be compared to the recording of a two-SM with oscillating phase [41]. Figures 12(a1) and 12(a2) illustrate the evolution of shot-to-shot DFT spectra over 500 cavity round trips, measured for a bi-SM and a tri-SM, respectively. Figures 12(b1) and 12(b2) display the corresponding multishot second-order autocorrelations traces, validating the soliton content of the above SMs. These results agree well with the numerical predictions presented in Fig. 5 when considering the basic level of characterization.

VII. CONCLUSION

We have presented a study that unveils important features that had not been reported so far concerning the dynamics of soliton molecules in mode-locked fiber lasers. We have developed the concept that the different solitons that make up a soliton molecule are deformable entities. We have shown that this approach requires the use of a characterization method that examines the individual behavior of each soliton of a molecule. Our analysis allowed us to highlight soliton molecules that inherently have an intensity profile that is dynamically distorted in an asymmetric way, including molecules whose energy is, on average, distributed unequally between the constituent solitons. We have also identified molecules that have intrinsically

a symmetric intensity profile, i.e., molecules whose energy is, on average, equally distributed between the constituent solitons. However, in the course of their propagation, those solitons can deform very asymmetrically, even with out-of-phase dynamics, which corresponds to an energy exchange process between soliton constituents. This illustrates the existence of a strong interaction taking place between adjacent solitons, such that in some situations their major parameters (energy, peak power, temporal width, spectral width) evolve asymmetrically.

Although there exist parameter regions where the laser generates bi- and tri-soliton molecules in a stationary state (i.e., without internal dynamics), in most parameter regions we found that the solitons in a bi- or tri-soliton molecule behaved like deformable entities interacting in an inelastic way.

This behavior constitutes a limit in the analogy that can be made between the soliton molecules in laser cavities and the matter molecules. Thus, we have presented a comprehensive theoretical analysis of the internal dynamics of different classes of soliton molecules, paving the way for future studies on the fine characterization of more complex soliton molecules, such as the molecular complexes discovered very recently [55].

Finally, we have presented some preliminary experimental results extending the observation to the case of tri-SM with oscillating phase dynamics. As pointed out in the Introduction, more advanced characterization will be required to retrieve the dynamics for the large number of internal variables involved in the detailed numerical analysis presented in this work.

ACKNOWLEDGMENTS

We acknowledge support from the Conseil Régional de Bourgogne, the CNRS, and the FEDER for their financial support.

-
- [1] N. Akhmediev and A. Ankiewicz, *Dissipative solitons in the complex Ginzburg-Landau and Swift-Hohenberg equations* (Springer, Berlin, 2005), pp. 1–17.
 - [2] P. Grelu and N. Akhmediev, *Nat. Photon.* **6**, 8492 (2012).
 - [3] W. Fu, L. G. Wright, P. Sidorenko, S. Backus, and F. W. Wise, *Opt. Express* **26**, 9432 (2018).
 - [4] N. N. Akhmediev, A. Ankiewicz, and J. M. Soto-Crespo, *Phys. Rev. Lett.* **79**, 4047 (1997).
 - [5] A. B. Grudinin and S. Gray, *J. Opt. Soc. Am. B* **14**, 144 (1997).
 - [6] P. Grelu, *Nonlinear Optical Cavity Dynamics: From Microresonators to Fiber Lasers* (WILEY-VCH Verlag GmbH & Co. KGaA, Weinheim, Germany, 2016).
 - [7] F. Sanchez, P. Grelu, H. Leblond, A. Komarov, K. Komarov, and M. Salhi, *Opt. Fib. Technol.* **20**, 562 (2014).
 - [8] D. Y. Tang, L. M. Zhao, B. Zhao, and A. Q. Liu, *Phys. Rev. A* **72**, 043816 (2005).
 - [9] F. W. Wise, A. Chong, and W. H. Renninger, *Laser Photon. Rev.* **2**, 58 (2008).
 - [10] F. Li, P. K. A. Wai, and J. N. Kutz, *J. Opt. Soc. Am. B* **27**, 2068 (2010).
 - [11] A. Haboucha, H. Leblond, M. Salhi, A. Komarov, and F. Sanchez, *Phys. Rev. A* **78**, 043806 (2008).
 - [12] B. G. Bale, J. N. Kutz, A. Chong, W. H. Renninger, and F. W. Wise, *J. Opt. Soc. Am. B* **25**, 1763 (2008).
 - [13] M. Alsaleh, T. Uthayakumar, E. Tchomgo Felenou, P. Tchofo Dinda, P. Grelu, and K. Porsezian, *J. Opt. Soc. Am. B* **35**, 276 (2018).
 - [14] X. Zhang, F. Li, K. Nakkeeran, J. Yuan, J. N. Kutz, and P. K. A. Wai, *IEEE J. Sel. Top. Quantum Electron.* **24**, 1101309 (2018).
 - [15] F. Guty, P. Grelu, N. Huot, G. Vienne, and G. Millot, *Electron. Lett.* **37**, 745 (2001).
 - [16] V. V. Afanasjev, B. A. Malomed, and P. L. Chu, *Phys. Rev. E* **56**, 6020 (1997).
 - [17] A. Grudinin, D. Richardson, and D. Payne, *Electron. Lett.* **28**, 67 (1992).
 - [18] A. K. Komarov and K. P. Komarov, *Opt. Commun.* **183**, 265 (2000).
 - [19] B. A. Malomed, *Phys. Rev. A* **44**, 6954 (1991).
 - [20] C. Paré and P.-A. Bélanger, *Opt. Commun.* **168**, 103 (1999).

- [21] D. Y. Tang, W. S. Man, H. Y. Tam, and P. D. Drummond, *Phys. Rev. A* **64**, 033814 (2001).
- [22] P. Grelu, F. Belhache, F. Gутty, and J.-M. Soto-Crespo, *Opt. Lett.* **27**, 966 (2002).
- [23] B.-F. Feng and B. A. Malomed, *Opt. Commun.* **229**, 173 (2004).
- [24] I. Gabitov, R. Indik, L. Mollenauer, M. Shkarayev, M. Stepanov, and P. M. Lushnikov, *Opt. Lett.* **32**, 605 (2007).
- [25] A. Hause, H. Hartwig, B. Seifert, H. Stolz, M. Böhm, and F. Mitschke, *Phys. Rev. A* **75**, 063836 (2007).
- [26] B. Ortaç, A. Zaviyalov, C. K. Nielsen, O. Egorov, R. Iliew, J. Limpert, F. Lederer, and A. Tünnermann, *Opt. Lett.* **35**, 1578 (2010).
- [27] X. Li, Y. Wang, W. Zhao, W. Zhang, X. Hu, C. Gao, H. Zhang, Z. Yang, H. Wang, X. Wang, C. Li, and D. Shen, *Opt. Commun.* **285**, 1356 (2012).
- [28] S. M. Alamoudi, U. Al Khawaja, and B. B. Baizakov, *Phys. Rev. A* **89**, 053817 (2014).
- [29] A. B. Moubissi, P. Tchofo Dinda, and S. Nse Biyoghe, *J. Opt.* **20**, 045503 (2018).
- [30] P. Grelu, S. Belhache, F. Gутty, and J. M. Soto-Crespo, *J. Opt. Soc. Am. B* **20**, 863 (2003).
- [31] H. Shi, Y. Song, C. Wang, L. Zhao, and M. Hu, *Opt. Lett.* **43**, 1623 (2018).
- [32] P. Rohrmann, A. Hause, and F. Mitschke, *Sci. Rep.* **2**, 866 (2012).
- [33] P. Rohrmann, A. Hause, and F. Mitschke, *Phys. Rev. A* **87**, 043834 (2013).
- [34] M. Grapinet and P. Grelu, *Opt. Lett.* **31**, 2115 (2006).
- [35] P. Wang, C. Bao, B. Fu, X. Xiao, P. Grelu, and C. Yang, *Opt. Lett.* **41**, 2254 (2016).
- [36] J. M. Soto-Crespo, P. Grelu, N. Akhmediev, and N. Devine, *Phys. Rev. E* **75**, 016613 (2007).
- [37] A. Zavyalov, R. Iliew, O. Egorov, and F. Lederer, *Phys. Rev. A* **79**, 053841 (2009).
- [38] S. Hamdi, A. Coillet, and P. Grelu, *Opt. Lett.* **43**, 4965 (2018).
- [39] J. M. Soto-Crespo and N. N. Akhmediev, *J. Opt. Soc. Am. B* **16**, 674 (1999).
- [40] K. Goda and B. Jalali, *Nat. Photon.* **7**, 102112 (2013).
- [41] K. Krupa, K. Nithyanandan, U. Andral, P. Tchofo-Dinda, and P. Grelu, *Phys. Rev. Lett.* **118**, 243901 (2017).
- [42] G. Herink, F. Kurtz, B. Jalali, D. R. Solli, and C. Ropers, *Science* **356**, 50 (2017).
- [43] X. Liu, X. Yao, and Y. Cui, *Phys. Rev. Lett.* **121**, 023905 (2018).
- [44] V. V. Afanasjev and N. Akhmediev, *Phys. Rev. E* **53**, 6471 (1996).
- [45] M. Liu, H. Li, A. P. Luo, H. Cui, W. Xu, and Z. C. Luo, *J. Opt.* **20**, 034010 (2018).
- [46] P. Ryczkowski, M. Narhi, C. Billet, J. M. Merolla, G. Genty, and J. M. Dudley, *Nat. Photon.* **12**, 221 (2018).
- [47] A. Tikan, S. Bielawski, C. Szewaj, S. Randoux, and P. Suret, *Nat. Photon.* **12**, 228 (2018).
- [48] P. Grelu and N. Akhmediev, *Opt. Express* **12**, 3184 (2004).
- [49] V. Roy, M. Olivier, F. Babin, and M. Piché, *Phys. Rev. Lett.* **94**, 203903 (2005).
- [50] M. Alsaleh, C. B. L. Mback, E. Tchomgo Felenou, P. Tchofo Dinda, P. Grelu, and K. Porsezian, *J. Opt.* **18**, 075501 (2016).
- [51] D. Anderson, *Phys. Rev. A* **27**, 3135 (1983).
- [52] P. Tchofo Dinda, A. B. Moubissi, and K. Nakkeeran, *Phys. Rev. E* **64**, 016608 (2001).
- [53] A. Kamagate, P. Grelu, P. Tchofo-Dinda, J. M. Soto-Crespo, and N. Akhmediev, *Phys. Rev. E* **79**, 026609 (2009).
- [54] G. Agrawal, *Nonlinear Fiber Optics*, Optics and Photonics (Elsevier Science, Amsterdam, 2012).
- [55] Z. Wang, K. Nithyanandan, A. Coillet, P. Tchofo-Dinda, and P. Grelu, *Nat. Commun.* **10**, 830 (2019).